PAPER

Morphology and structure controlled growth of one-dimensional AlN nanorod arrays by hydride vapor phase epitaxy

Susu Kong,[a] Hongyuan Wei,*[a] Shaoyan Yang,*[a] Huijie Li,[a] Yuxia Feng,[a] Zhen Chen,[a] Xianglin Liu,[ab] Lianshan Wang[a] and Zhanguo Wang[a]

Well-aligned one-dimensional aluminium nitride (AlN) nanorod arrays were grown on sapphire substrate by hydride vapor phase epitaxy (HVPE) with a temperature range from 750 °C to 900 °C. No template or catalyst was used during the whole procedure. The crystal structure and morphology of the AlN nanorods were investigated by X-ray diffraction, Raman spectroscopy, scanning and transmission electron microscopy. All the AlN nanorods were preferentially grown along the *c*-axis and perpendicular to the sapphire substrate. The morphology of single crystal AlN nanorods was closely related to growth temperature and V/III. Different stages of the growth were studied in detail and a vapor–solid growth mechanism with an anisotropic growth rate caused by limited migration of adatoms on the surface of the substrate explains the formation of AlN nanorods.

Introduction

One-dimensional (1D) nanostructure materials have attracted tremendous attention for their potential applications in devices at the nanoscale.[1–3] Owing to the unique properties of nanostructured materials, devices based on these materials will have enhanced performance.[4,5] Group III-nitrides have been regarded as the most important wide band gap semiconductors, their superior properties in light emission covering from the near-IR to the UV region, excellent thermal conductivity and high chemical resistance make them widely applied in optoelectronic and electronic devices.[6,7] Efforts have been made on fabricating corresponding devices at nanoscale, for example, lasers based on III-nitride nanowires.[8,9] Aluminium nitride (AlN) possesses the largest band gap (6.2 eV) in III-nitrides, extraordinaire thermal conductivity (3.2 W cm^{-1} K^{-1}), high melting temperature (3000 °C), excellent mechanical strength[10] and low electron affinity.[11] These distinctive properties making AlN 1D nanostructures material potential applications on NEMS,[12] hydrogen storage,[13] filed emission application[14] and gas sensor.[15]

Up to present, AlN 1D nanostructures have been growth by many groups using chemical vapor deposition (CVD),[16–19] metalorganic chemical vapor deposition (MOCVD)[20,21] and some other methods,[22] but using hydride vapor phase epitaxy (HVPE) is rarely seen.[23] High growth temperature (>1000 °C),[16,24] long

growth duration (>1 hour)[17,25,26] or catalyst[20,27] are often needed for AlN nanostructures material growth using CVD or MOCVD. AlN nanorods with different diameters were grown by HVPE before and the decreasing of growth rate was attributed to the drop in the reactant gases concentration.[23] In the presented study, we present a catalyst-free and fast growth method to fabricate well-aligned AlN 1D nanostructure arrays at relatively low temperature. The AlN 1D nanostructure arrays were directly grown on sapphire substrate. The influence of growth temperature and V/III on the morphology and structure of AlN nanostructures was investigated. The different stages of the growth were studied by altering the growth time at certain temperature. Anisotropic growth rate caused by limited migration of adatoms on the surface of the substrate is proposed to explain the formation of AlN nanostructures. Furthermore, this AlN nanorods growth method can be applied to lower growth temperatures[28] or to different substrates[29] like GaN.
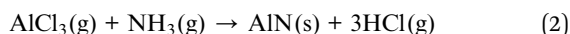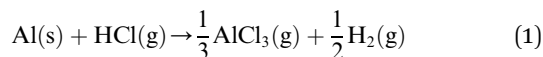
Experimental details

AlN 1D nanostructures were grown on *c*-plane sapphire substrates in a home-build horizontal HVPE system. There are two zones in this system, namely source zone and reaction zone, both of them have a separated heating system. Al metal pellets (5 N grade) were placed in a quartz boat in the source zone, HCl was introduced into the source zone by carrying gas, then AlCl$_3$ was formed *in situ* by reaction between Al and HCl (reaction (1)). AlCl$_3$ was transported and mixed with NH$_3$ in reaction zone and AlN 1D nanostructures were deposited on the sapphire substrate by reaction between AlCl$_3$ and NH$_3$ in N$_2$ atmosphere (reaction (2)) at the downstream region of the reaction zone. In

[a]Key Laboratory of Semiconductor Materials Sciences, Institute of Semiconductors, Chinese Academy of Sciences, Beijing, People's Republic of China. E-mail: why@semi.ac.cn; sh-yyang@semi.ac.cn

[b]LatticePower Corporation, Nanchang, People's Republic of China

our experiments, the temperature of source zone was fixed at 550 °C to make sure reaction (1) is predominant and $AlCl_3$ was the main $AlCl_x$ production.[30] The temperature of reaction zone was set between 750 °C–900 °C. N_2 was served as the carrying gas. The flow rate of HCl was fixed at 100 sccm and total gas flow rate was 3600 sccm. The pressure of the whole HVPE system was keep at 100 Torr.

$$Al(s) + HCl(g) \rightarrow \frac{1}{3}AlCl_3(g) + \frac{1}{2}H_2(g) \qquad (1)$$

$$AlCl_3(g) + NH_3(g) \rightarrow AlN(s) + 3HCl(g) \qquad (2)$$

The crystal structure and morphology of the AlN 1D nanostructures were characterized by X-ray diffraction (XRD: Rigaku SmartLab, Cu Kα), field emission scanning electron microscopy (FE-SEM: FEI NOVA NanoSEM 650 and Zeiss Merlin), transmission electron microscopy (TEM: FEI Tecnai G2 F20) and Raman spectroscopy (LabRAM HR Evolution).

Results and discussion

Fig. 1 shows the typical XRD patterns of AlN samples grown at different temperature. The flow rate of NH_3 was keep at 500 sccm and all the AlN nanostructures were grown for 30 minutes. The diffraction peaks around 36.04° are correspond to (0002) diffraction peak of wurtzite-type hexagonal AlN. The predominant (0002) diffraction peaks indicate that the AlN nanostructures are preferential grown along c-axes. The (10$\bar{1}$1) diffraction peaks can be seen at full temperature range, while (10$\bar{1}$0) diffraction peak can only be seen at 750 °C. Nevertheless, the intensity of (10$\bar{1}$0) and (10$\bar{1}$1) diffraction peaks are week comparing to (0002) diffraction peak. The X-ray rocking curves of the (0002) plane, the insert (a) of Fig. 1, show a broad peak centred around 18°. This indicates that the as-grown AlN nanostructures are preferentially oriented along the c-axis direction and nearly perpendicular to the substrate. The epitaxy relationship between the AlN nanorods and sapphire is not obviously because of the low growth temperature, the in-plane

orientation is disorderly according to the phi scan of (10$\bar{1}$1) plane (inset (b) of Fig. 1).

The morphology of AlN nanostructures grown at different temperature was studied by FE-SEM. In our experiment, the growth temperature is the key factor affecting the shape of AlN nanostructures. For the growth temperature of 750 °C, well-aligned and vertical AlN nanorods can be seen in Fig. 2a and b. Although the bottom of AlN layer has coalesced, separated and high-density AlN nanorods can be seen at the top of AlN layer. These AlN nanorods are about 2 ± 0.2 μm long with shrinking diameter along the growth direction. When the temperature was increased to 800 °C, the diameter of AlN nanorods increased, as shown in Fig. 2c. The average diameter and length of rods are 250 ± 50 nm and 2 ± 0.2 μm, respectively. Hexagonal facets can be seen at the top of AlN nanorods in Fig. 2d inset. The growth rate of the AlN nanorods grown at 750 °C and 800 °C was about 4 μm h^{-1}. A further increase of the growth temperature lead to AlN hexagonal columns (Fig. 2e and f). The average diameter and length of these columns are 2 ± 0.18 μm and 3 ± 0.1 μm, respectively. The density of the AlN columns is lower than the AlN nanorods grown at 750 °C and 800 °C. Hexagonal defect can be seen on the top of column, which might be etched by HCl.[31]

The morphology of AlN nanorods was also affected by the V/III ratio. In our experiments, the flow rate of NH_3 was increased to obtain different V/III. Fig. 3 reports the post-growth SEM
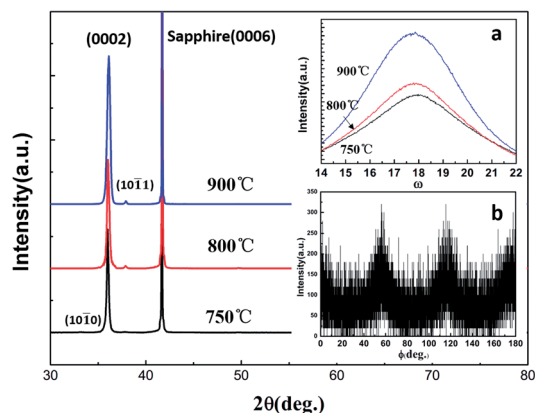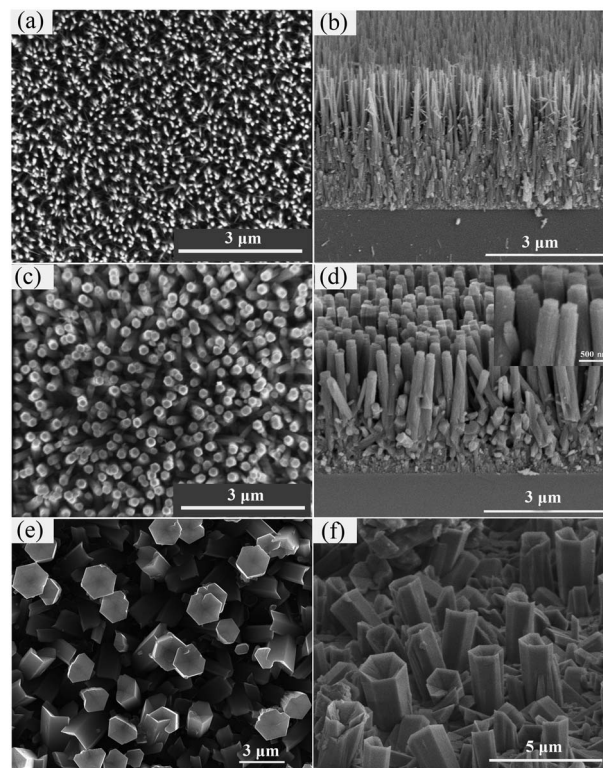

Fig. 2 Typical SEM images of the AlN nanorods grown with temperature at (a) and (b) 750 °C, (c) and (d) 800 °C, (e) and (f) 900 °C, respectively. Inset in (d) is an enlarged image of the top of AlN nanorods grown at 800 °C.
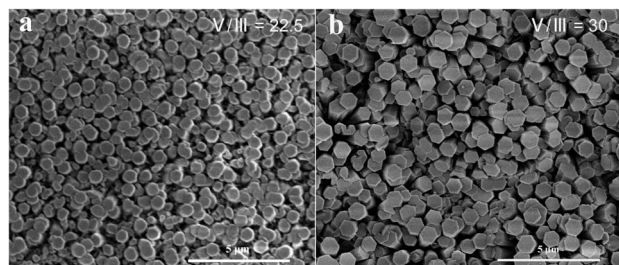

Fig. 1 XRD patterns of the AlN samples grown at different temperature. Inset (a) is the rocking curve of (0002) plane, (b) is the phi scan of (10$\bar{1}$1) plane of the AlN nanorods grown at 800 °C.

Fig. 3 SEM images of the AlN nanorods grown with V/III at (a) 22.5, (b) 30.

Fig. 5 (a) TEM image, (b) corresponding HR-TEM image and the FFT pattern (inset) of one single AlN nanorod grown at 750 °C.

images of AlN nanorods grown with different V/III ratio at 800 °C for 30 minutes. For high V/III ratios of 30 and 22.5, the diameter of AlN nanorods was larger than those grown with the V/III ratio of 15 (Fig. 3c). When the V/III was increased to 22.5, the average diameter of AlN nanorods was increased to 550 nm (Fig. 3a). For a further increase of the V/III to 30, the shape of AlN nanorods changed into hexagonal columns and was similar to the AlN nanorods grown at 900 °C except for much smaller diameter and higher density (Fig. 3b).

As the diameter of AlN columns grown at 900 °C was micron level, we focus on the AlN nanorods grown at 750 °C and 800 °C, further structure characterization of the AlN nanorods was carried out by Raman spectroscopy and transmission electron microscope (TEM). The Raman spectrum of the AlN nanorods was recorded at room temperature using a 532 nm solid state laser as the excitation source. There are six Raman-active modes, A_1 (TO), A_1 (LO), E_1 (TO), E_1 (LO), E_2 (high) and E_2 (low), in the first-order Raman scattering of wurtzite-type AlN. The E_2 (high), E_2 (low) and A_1 (LO) are Raman-active modes in the backscattering configuration. However, other Raman modes may appear since not all the AlN nanorods were strictly vertical to the substrate.[32] Fig. 4 is the Raman spectra of the AlN nanorods grown at 750 °C and 800 °C, the peaks located at 250, 613, 653 and 890 cm^{-1} can be assigned to E_2 (low), A_1 (TO), E_2 (high) and A_1 (LO), respectively. These are in agreement with those reported in the literatures.[33,34]

AlN nanorod with base diameter of 50 nm and apex diameter of 20 nm can be seen in Fig. 5a. Fig. 5b is the HRTEM image of one
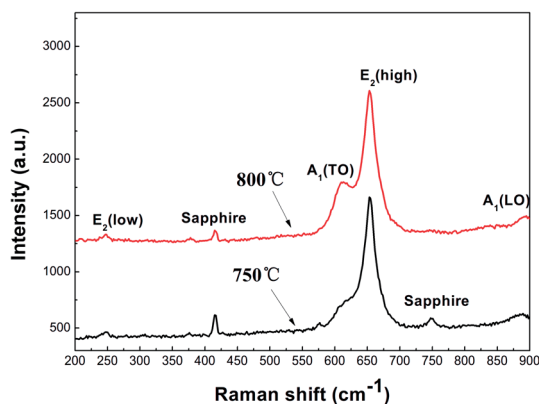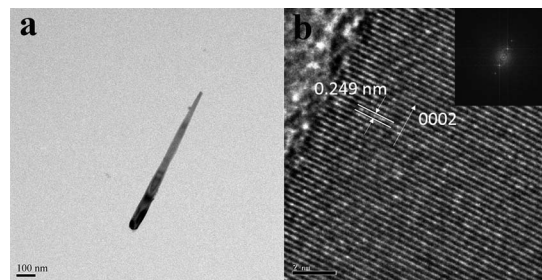
part of the nanorod. The interplanar spacing of 0.249 nm is in agree with those of (0002) plane of AlN. Low-magnification TEM image of AlN nanorod grown at 800 °C is shown in Fig. 6a, a decrease of diameter at the top of the rod can be seen, which is consistent with SEM image (Fig. 2d). The selected-area electron diffraction (SAED) pattern, which was taken along [010] zone axis, can be indexed as wurtzite-type hexagonal AlN and matches well with the corresponding HRTEM image (Fig. 6c). The interplanar spacing of (0001) and (10Ī0) planes is 0.499 nm and 0.269 nm, respectively. The results of Raman spectra and TEM indicate that the AlN nanorods grown at 750 °C and 800 °C are in good crystal quality and preferential grow along the [0002] direction.

In order to investigate the growth mechanism of the AlN nanorods, experiments were taken with different growth time at 800 °C with V/III of 15. The growth time was set at 30 seconds, 2 minutes, 5 minutes and 15 minutes, respectively. Fig. 7a is the cross-section SEM image of the AlN nanorods grown for 30 s, rod-like structures can be clearly seen even with such short time. That means AlN nanorods growth started at the initial stage of growth. Fig. 6b–d show the AlN nanorods grown for 2 min, 5 min and 15 min, respectively. When the growth time was increased, the length of nanorods increased roughly from 120 nm to 1.5 μm, while the diameter of nanorods only increased roughly from 30 nm to 135 nm.

As we did not apply Ni, Au or any other metal as catalyst in our experiment, the growth mechanism of AlN nanorods should
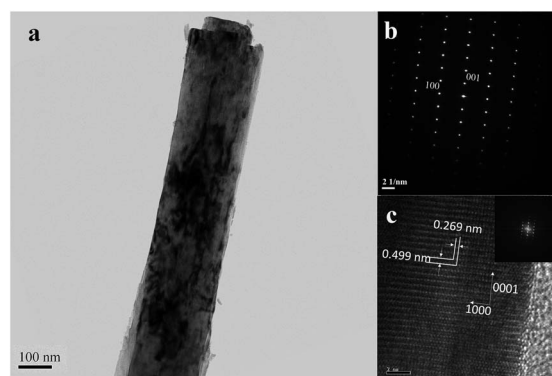

Fig. 4 Raman spectra of AlN nanorods grown at 750 °C and 800 °C.

Fig. 6 (a) TEM image, (b) SAED pattern, and (c) corresponding HR-TEM image and FFT pattern (inset) of one single AlN nanorod grown at 800 °C.
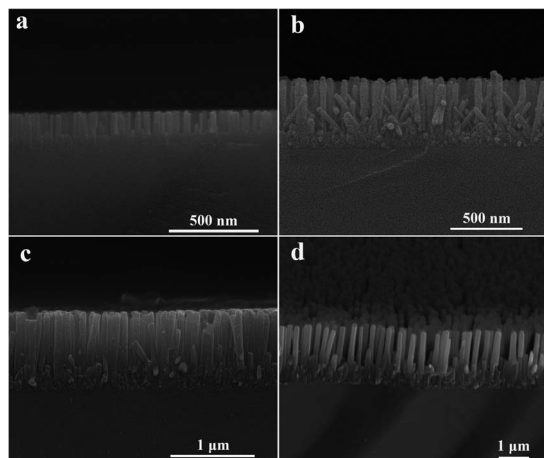
Fig. 7 Typical SEM images of the AlN nanorods grown at 800 °C with growth time set at (a) 30 seconds, (b) 2 minutes, (c) 5 minutes, and (d) 15 minutes.

be vapor–solid (VS) mechanism. Briefly, the gaseous source species transported to the surface of sapphire and reacted to form solid state AlN. Those solid state AlN absorbed onto the sapphire surface and AlN nucleus centers were then formed by the migration of those adatoms. According to van der Drift's evolutionary selection in growth orientation,[35] [0002] direction, which is normal to the substrate, will survival during the competition with other growth directions, so the AlN nanorods grown along [0002] direction was preferential. Meanwhile, the strong covalent Al–N bonds restricted the migration of adatoms on the surface of substrate at low temperature, so the lateral growth of AlN nucleus and nanorods was restrained.[36] Fig. 8 shows the growth rate of different directions as a function of the growth time at 800 °C. The feature sizes were determined from SEM measurements of the average diameter and length of AlN nanorods grown at different time. It's clearly shows that the vertical growth is far greater than lateral grow rate. AlN 1D nanostructures growth occurred with this anisotropic growth rate between vertical and lateral growth.
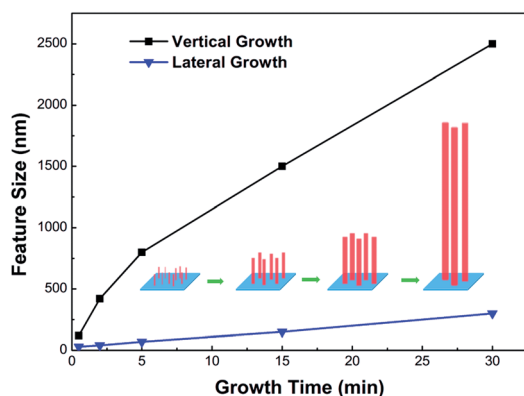

Fig. 8 Growth rate of vertical and lateral direction as function of growth time. Inset is the schematic that illustrates the formation of AlN nanorods.

The migration of adatoms is closely related to growth temperature, the surface diffusion length of adatoms, L_s, can be expressed as:

$$L_s = \sqrt{2D\tau}$$

where D is the diffusion coefficient and τ is the life time of the adatoms between the absorption and desorption. Diffusion coefficient was the measure of species mobility and proportional to $\exp(-E_{diff}/K_B T)$, where E_{diff} is the activation energy for surface diffusion and K_B is the Boltzmann constant.[37] The diffusion length of Al adatoms on the AlN surface is approximately 6.8 nm at 700 °C and increases as the growth temperature rises.[38] When the growth temperature was set at 750 °C, the migration of adatoms was so weak that the diameter shrunk along the [0002] direction. This shrinkage of diameter was a result of Ehrlich–Schwoebel barrier and consistent with the previous study.[16] At 800 °C, the hexagonal facets on the top of AlN nanorods were left when we cut out the supply of the source species (Fig. 2d inset), little hexagonal columns were grown at first, but insufficient lateral migration of adatoms made the hexagonal facets change into pillar facets during the subsequent growth. When the growth temperature was increased to 900 °C, hexagonal facets can be maintained due to sufficient lateral migration at higher growth temperature, the diameter of the AlN columns was much larger than those grown at 750 °C and 800 °C.

The supersaturation γ also plays an important role for the growth process. The supersaturation represents the progress of the reaction with respect to equilibrium.[39] In the present investigations, supersaturation γ can be expressed as:

$$\gamma = \frac{P_{\text{Al species}} \times P_{\text{N species}}}{P_{\text{eq Al species}} \times P_{\text{eq N species}}}$$

where P is the partial pressure of reaction species and P_{eq} is the equilibrium partial pressure of Al and N species.[40] At high V/III ratio, the local supersaturation γ is high enough, because of high NH_3 partial pressure, to generate plenty of AlN nucleus centers for planar growth and the lateral growth was strengthened under this circumstance. So the diameter of AlN nanorods increased with the increasing of V/III ratio. When the V/III ratio was increased to 30, the AlN hexagonal columns can be maintained due to the high local supersaturation.

Conclusions

In conclusion, we report a fast and temperature controlled growth method of single crystal AlN nanorods. Well-aligned AlN nanorod arrays with preferential c-axis orientation have been successfully grown by HVPE without any catalyst or template. XRD, Raman and TEM results indicating AlN nanorods are single crystalline and in good crystal quality. With an increase in the growth temperature, AlN nanorods with different diameter and density have been grown. The increase of the diameter of AlN nanorods are due to the enhanced migration of adatoms at higher temperature. The morphology of AlN nanorods was also affected by V/III, high V/III is beneficial for lateral growth in our experiments. Different stages of the growth was discussed.

It was found that the vertical growth rate was far great than the lateral growth. A VS growth model with anisotropic growth rate was proposed to explain the formation of AlN nanorods.

Acknowledgements

Notes and references

1 P. Y. Y. Xia, Y. Sun, Y. Wu, B. Mayers, B. Gates, Y. Yinl, F. Kim and H. Yan, *Adv. Mater.*, 2003, **15**, 353.

2 S. Barth, F. Hernandez-Ramirez, J. D. Holmes and A. Romano-Rodriguez, *Prog. Mater. Sci.*, 2010, **55**, 563–627.

3 Z. L. Wang and J. H. Song, *Science*, 2006, **312**, 242–246.

4 H. D. Espinosa, R. A. Bernal and M. Minary-Jolandan, *Adv. Mater.*, 2012, **24**, 4656–4675.

5 S. F. Li and A. Waag, *J. Appl. Phys.*, 2012, **111**, 071101.

6 S. Nakamura, T. Mukai and M. Senoh, *Appl. Phys. Lett.*, 1994, **64**, 1687–1689.

7 S. J. Pearton, B. S. Kang, S. K. Kim, F. Ren, B. P. Gila, C. R. Abernathy, J. S. Lin and S. N. G. Chu, *J. Phys.: Condens. Matter*, 2004, **16**, R961–R994.

8 S. Gradečak, F. Qian, Y. Li, H.-G. Park and C. M. Lieber, *Appl. Phys. Lett.*, 2005, **87**, 173111.

9 S. Arafin, X. H. Liu and Z. T. Mi, *J. Nanophotonics*, 2013, **7**, 074599.

10 L. Liu and J. H. Edgar, *Mater. Sci. Eng., R*, 2002, **37**, 61–127.

11 M. Kasu and N. Kobayashi, *Appl. Phys. Lett.*, 2000, **76**, 2910.

12 G. Guisbiers and L. Buchaillot, *J. Phys. D: Appl. Phys.*, 2008, **41**, 172001.

13 Q. Wang, Q. Sun, P. Jena and Y. Kawazoe, *ACS Nano*, 2009, **3**, 621–626.

14 F. Liu, Z. J. Su, F. Y. Mo, L. Li, Z. S. Chen, Q. R. Liu, J. Chen, S. Z. Deng and N. S. Xu, *Nanoscale*, 2011, **3**, 610–618.

15 Z. Zhou, J. Zhao, Y. Chen, P. Schleyer and Z. Chen, *Nanotechnology*, 2007, **18**, 424023.

16 S.-C. Shi, S. Chattopadhyay, C.-F. Chen, K.-H. Chen and L.-C. Chen, *Chem. Phys. Lett.*, 2006, **418**, 152–157.

17 J. Yang, T. W. Liu, C. W. Hsu, L. C. Chen, K. H. Chen and C. C. Chen, *Nanotechnology*, 2006, **17**, S321–S326.

18 X. Song, Z. Guo, J. Zheng, X. Li and Y. Pu, *Nanotechnology*, 2008, **19**, 115609.

19 F. Zhang, Q. Wu, X. Z. Wang, N. Liu, J. Yang, Y. M. Hu, L. S. Yu and Z. Hu, *Vacuum*, 2012, **86**, 833–837.

20 J. Su, G. Cui, M. Gherasimova, H. Tsukamoto, J. Han, D. Ciuparu, S. Lim, L. Pfefferle, Y. He, A. V. Nurmikko, C. Broadbridge and A. Lehman, *Appl. Phys. Lett.*, 2005, **86**, 013105.

21 V. Cimalla, C. Foerster, D. Cengher, K. Tonisch and O. Ambacher, *Phys. Status Solidi B*, 2006, **243**, 1476–1480.

22 W. W. Lei, D. Liu, P. W. Zhu, Q. S. Wang, G. Liang, J. Hao, X. H. Chen, Q. L. Cui and G. T. Zou, *J. Phys. Chem. C*, 2008, **112**, 13353–13358.

23 Y. K. Byeun, R. Telle, S. H. Jung, S. C. Choi and H. I. Hwang, *Chem. Vap. Deposition*, 2010, **16**, 72–79.

24 Q. Wu, Z. Hu, X. Z. Wang, Y. N. Lu, K. F. Huo, S. Z. Deng, N. S. Xu, B. Shen, R. Zhang and Y. Chen, *J. Mater. Chem.*, 2003, **13**, 2024–2027.

25 Q. Zhao, H. Zhang, X. Xu, Z. Wang, J. Xu, D. Yu, G. Li and F. Su, *Appl. Phys. Lett.*, 2005, **86**, 193101.

26 C. Liu, Z. Hu, Q. Wu, X. Wang, Y. Chen, H. Sang, J. Zhu, S. Deng and N. Xu, *J. Am. Chem. Soc.*, 2005, **127**, 1318–1322.

27 H. Cui, Y. Sun and C. X. Wang, *CrystEngComm*, 2013, **15**, 5376.

28 E. Nakamura, K. Ueno, J. Ohta, H. Fujioka and M. Oshima, *Appl. Phys. Lett.*, 2014, **104**, 051121.

29 J. H. Choi, A. Zoulkarneev, S. I. Kim, C. W. Baik, M. H. Yang, S. S. Park, H. Suh, U. J. Kim, H. Bin Son, J. S. Lee, M. Kim, J. M. Kim and K. Kim, *Nat. Photonics*, 2011, **5**, 763–769.

30 Y. Kumagai, T. Yamane, T. Miyaji, H. Murakami, Y. Kangawa and A. Koukitu, *Phys. Status Solidi C*, 2003, 2498–2501.

31 Y. S. Won, Y. S. Kim, O. Krylouk and T. J. Anderson, *J. Cryst. Growth*, 2008, **310**, 3735–3740.

32 T. Prokofyeva, M. Seon, J. Vanbuskirk, M. Holtz, S. Nikishin, N. Faleev, H. Temkin and S. Zollner, *Phys. Rev. B: Condens. Matter Mater. Phys.*, 2001, **63**, 125313.

33 H. Harima, *J. Phys.: Condens. Matter*, 2002, **14**, R967–R993.

34 J. G. Tischler and J. A. Freitas, *Appl. Phys. Lett.*, 2004, **85**, 1943.

35 A. Vanderdr, *Philips Res. Rep.*, 1967, **22**, 267–288.

36 J. Zheng, Y. Yang, B. Yu, X. B. Song and X. G. Li, *ACS Nano*, 2008, **2**, 134–142.

37 Y. Kangawa, T. Akiyama, T. Ito, K. Shiraishi and T. Nakayama, *Materials*, 2013, **6**, 3309–3360.

38 X. Q. Shen, H. Matsuhata, T. Ide and M. Shimizu, *J. Appl. Phys.*, 2012, **111**, 103529.

39 K. Lekhal, G. Avit, Y. Andre, A. Trassoudaine, E. Gil, C. Varenne, C. Bougerol, G. Monier and D. Castelluci, *Nanotechnology*, 2012, **23**, 405601.

40 A. Claudel, E. Blanquet, D. Chaussende, M. Audier, D. Pique and M. Pons, *J. Cryst. Growth*, 2009, **311**, 3371–3379.